Chinese Journal of Chemical Engineering 69 (2024) 122–134

Contents lists available at ScienceDirect

Chinese Journal of Chemical Engineering

journal homepage: www.elsevier.com/locate/CJChE

Full Length Article

A strategy for strengthening chaotic mixing of dual shaft eccentric mixers by changing non-Newtonian fluids kinetic energy distribution

Songsong Wang [1, 2], Tong Meng [1, 2], Qian Zhang [1], Changyuan Tao [1, 2], Yundong Wang [3], Zequan Li [1], Zuohua Liu [1, 2, *]

[1] *School of Chemistry and Chemical Engineering, Chongqing University, Chongqing 400044, China*
[2] *State Key Laboratory of Coal Mine Disaster Dynamics and Control, Chongqing 400044, China*
[3] *Department of Chemical Engineering, Tsinghua University, Beijing 100084, China*

A R T I C L E I N F O

Article history:
Received 13 October 2023
Received in revised form
26 January 2024
Accepted 31 January 2024
Available online 28 February 2024

Keywords:
Dual shaft
"U-shaped" baffle
Flow pattern
Mixing time
Power demand

A B S T R A C T

Efficiently modulating the velocity distribution and flow pattern of non-Newtonian fluids is a critical challenge in the context of dual shaft eccentric mixers for process intensification, posing a significant barrier for the existing technologies. Accordingly, this work reports a convenient strategy that changes the kinetic energy to controllably regulate the flow patterns from radial flow to axial flow. Results showed that the desired velocity distribution and flow patterns could be effectively obtained by varying the number and structure of baffles to change kinetic energy, and a more uniform velocity distribution, which could not be reached normally in standard baffle dual shaft mixers, was easily obtained. Furthermore, a comparative analysis of velocity and shear rate distributions is employed to elucidate the mechanism behind the generation of flow patterns in various dual-shaft eccentric mixers. Importantly, there is little difference in the power number of the laminar flow at the same Reynolds number, meaning that the baffle type has no effect on the power consumption, while the power number of both unbaffle and U-shaped baffle mixing systems decreases compared with the standard baffle mixing system in the transition flow. Finally, at the same rotational condition, the dimensionless mixing time of the U-shaped baffle mixing system is 15.3% and 7.9% shorter than that of the standard baffle and the unbaffle mixing system, respectively, which shows the advantage of the U-shaped baffle in stirring rate.

1. Introduction

Non-Newtonian fluids play a significant role in the chemical industry and are widely used in the production of food, paint, biopharmaceuticals and cosmetics. However, due to its special shear-thinning rheological characteristics [1–3], the viscosity distribution in agitated tanks is not uniform, and it is easy to form flow dead zones, which leads to many problems, such as wall fouling, low heat, mass transfer efficiency and high mixing time [4–8]. Therefore, achieving efficient mixing of non-Newtonian fluids is crucial for increasing production yield and enhancing product quality.

With the advancement of chaos theory, experts have recognized the potential of chaotic phenomena in achieving the mixing of laminar fluids. Aref [9] and Ottino [10] first proposed the chaotic mixing theory and verified the superiority of the two-dimensional mixing regime. Subsequently, the application was extended to three dimensions, leading to the proposal of chaotic mixing [11,12], which marked a significant milestone in the field of mixing research. Based on the space-time chaotic mixing theory, scholars worldwide have put forward various methods to enhance fluid mixing. One approach involves breaking away from conventional steady-state mixing, known as temporal chaotic mixing. Examples include variable speed mixing [13], forward and reverse mixing [14], and other techniques aimed at disrupting the periodicity of fluid flow and inducing fluid chaos. Another approach focuses on improving the design and arrangement of paddles, referred to as spatial chaotic mixing. These methods include rigid-flexible combination impellers [15–17], eccentric shaft mixers [18,19], multilayer combination impellers [20], staggered agitators [21],

* Corresponding author.
E-mail address: liuzuohua@cqu.edu.cn (Z. Liu).

https://doi.org/10.1016/j.cjche.2024.01.016
1004-9541/

multi-shaft mixers [22–24], and other strategies to disrupt the spatial symmetry of fluid flow.

The impeller is one of the core components in mixers, and its type, size, number, and rotation speed significantly impact the flow field and mixing performance. Scholars have developed various innovative impellers to achieve non-steady state energy transfer in the flow field, enhance the complexity of the flow field, improve break symmetry, and improve mixing efficiency. Luan *et al.* [25,26] dislocated the blades of the six-bent blade (6BT) impeller up and down and named it the impeller of a perturbed six-bent-bladed turbine (6PBT). The 6PBT impeller addressed symmetry issues in non-Newtonian fluid mixing, resulting in substantial improvements in mixing efficiency. Liu *et al.* [15–17] inspired by the biomimetic principle of fish fins, introduced a novel rigid-flexible combination impeller. By employing flexible and variable blades that induce irregular disturbances in the fluid, they effectively enhance mass transfer between fluids, induce chaotic flows, eliminate fluid dead zones, and improve laminar mixing characteristics. Yang *et al.* [27] developed a Rushton impeller equipped with flexible blades. Through a combination of experimental and computational fluid dynamics (CFD) approaches, the flexible Rushton impeller exhibited strong adaptability, enhanced radial momentum transfer, and reduced macro mixing time by 29.4% compared to standard Rushton impellers. Gu *et al.* [28,29] invented a novel self-similarity impeller agitator, which has been applied in research on pseudoplastic fluid mixing. The results demonstrated that the self-similar structure design of the impeller could effectively enlarge the well-mixed regions and improve the mixing efficiency of the pseudoplastic fluid mixing process. Luo *et al.* [30] invented a novel long-short blades (LSB) agitator, which has been applied in research on gas–liquid two-phase mixing. Experimental results demonstrated that the LSB agitator improved bubble distribution and facilitated effective gas–liquid mass transfer.

Furthermore, altering the impeller's motion pattern can enhance mixing efficiency, directly benefiting practical production processes. Kordas *et al.* [31] introduced a stirred reactor equipped with reciprocating blades and investigated the impact of rotational speed on mixing time and power consumption. The findings demonstrated that the reciprocating stirred effectively induced fluid chaos and reduced isolation zones. Gao *et al.* [13] conducted particle image velocimetry (PIV) experiments to compare the radial velocity distribution in laminar flow between variable-speed and constant-speed stirred. The results revealed that variable-speed stirring exhibited superior flow field velocity distribution. Building upon chaos control theory, Zhang *et al.* [32] proposed employing a Chua circuit to generate chaotic signals for motor control, resulting in chaotic rotation of the impeller. Chaotic stirring was observed to effectively dismantle isolated mixing regions, leading to a remarkable enhancement in mixing efficiency within the stirred tank. Lamberto *et al.* [33] induced chaotic flow by periodically rotating the impeller blades in a square wave pattern. By employing high-speed camera technology, the study demonstrated a gradual reduction of isolated mixing regions above and below the impeller during the cyclic rotation of the blades.

The above-mentioned studies mainly focused on the types and motion behavior of impellers. However, as one of the important internal components of a stirred tank, the baffle also plays a significant role in controlling the motion behavior of the flow field and inducing fluid instability in the wall regions. Moreover, it has been shown that the “standard baffle” is not suitable for all mixing conditions, and the flow dead zone is easily formed behind the baffle, and in some cases, the non-standard baffle is superior [34–36]. Xiong *et al.* [37] investigated the power consumption and solid–liquid suspension characteristics of three systems: the unbaffled stirred tank, the traditional baffled stirred tank, and the punched baffled stirred tank (Pun-BST). The results showed that the Pun-BST system exhibited significantly improved mixing characteristics. Sirasitthichoke *et al.* [38] studied the effect of baffle curvature on the velocity, flow pattern, and power consumption in the stirred tank. It was found that, compared to straight baffles, curved baffles could generate a well-defined mixing region and stronger radial fluid flow.

In the present study, based on the initial condition sensitivity of chaos theory, a strategy of regulating the kinetic energy distribution to strengthen fluid chaotic mixing is established by a novel U-shaped baffle combined with a dual shaft. Power demand performance in different dual-shaft eccentric mixers was first compared. Then, the velocity distribution laws were investigated and tried to find the inherent mass transfer mechanism in different baffle mixing systems. Besides, the effects of rotational speed on the average shear rate were studied in three different mixing systems. Finally, the mixing performance and mass transfer behavior in the U-shaped baffle stirred tank were revealed, and a new prediction model for the dimensionless mixing time was developed.

2. Experimental

2.1. Experimental apparatus

The dual-shaft eccentric experimental apparatus and the applied measurement techniques are shown in Fig. 1. The main devices include a data collection and control system, a high-speed camera (5F04 M, Revealer, China), stirred equipment, and an electromotor. The rotational speed and direction of the two shafts are driven by separate motors, and each shaft was equipped with a rotary torque sensor to continuously measure the torque (HX-90D, Huaxin Electromechanical, China). As non-Newtonian fluids, carboxyl methyl cellulose (CMC) was used in mixing experiments. The structure of the cylindrical flat-bottomed stirred tanks (diameter is $T = 240$ mm, liquid height is $H = 360$ mm), as shown in Fig. 1(b). Fig. 1(c) shows the three kinds of mixing systems, namely the vertical baffle vessel, the unbaffled vessel, and the “U-shaped” parallel baffle vessel. Two impellers used in the experiment were a rushton turbine (RT) and a pitched blade down-pumping rushton turbine ($PBRT_D$) (diameter is $D = T/3$). The inclined angles (θ) of $PBRT_D$ were 45°. The blade thickness of the impellers was 2 mm.

The dimensions of various parts are given in Table 1.

2.2. Materials and measurement strategy

2.2.1. Materials

In the present study, the mass fraction of 0.5% CMC solution was employed in chaotic mixing experiments. The density and rheological parameters are shown in Table 2 [22,23].

The investigated CMC fluids are typical non-Newtonian fluids; the rheological properties of the shear-thinning fluids could be described by the power-law model [39,40].

$$\tau = K\dot{\gamma}^{n} \tag{1}$$

$$\mu_a = K\dot{\gamma}^{n-1} \tag{2}$$

where $\dot{\gamma}$ is the shear rate, s^{-1}; μ_a is the apparent viscosity, Pa·s.

The viscosity of non-Newtonian fluid is a power-law function of shear rate. In this study, the value of the Reynolds number can be obtained as follows [41,42]:

$$Re = \frac{\rho N D^2}{\mu_a} = \frac{\rho N^{(2-n)} D^2}{K k_s^{n-1}} \tag{3}$$

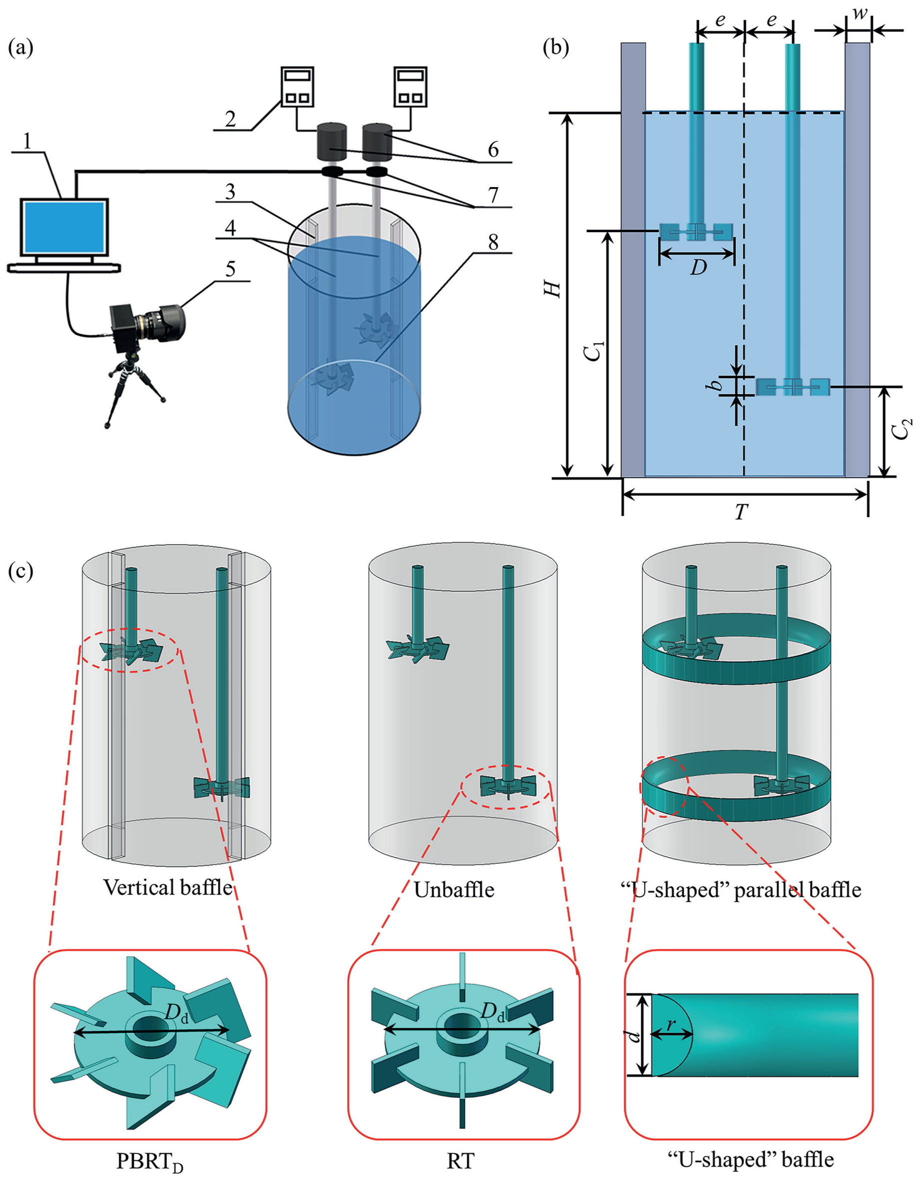

Fig. 1. Schematic diagrams of the stirred experimental system: (a) experimental apparatus; (b) dual shaft eccentric mixer; (c) three vessels. 1—data collection and control system; 2—frequency modulator; 3—baffle; 4—stirred shaft; 5—high speed camera; 6—electromotor; 7—torque sensor; 8—tank.

Table 1
Dimensions of various parts in the vessel

b/mm	d/mm	r/mm	H/mm	T/mm	C_1/H	C_2/H	D_d/T	e/T
16	30	15	360	240	0.7	0.2	0.25	0.24

Table 2
The rheological parameter of CMC solution

Concentration, w_t/%	Density, ρ/ kg·m^{-3}	Consistency coefficient, K/ Pa·s^n	Power law index, n
0.5	985	0.305	0.878

where D is the impeller diameter, m; k_s is the Metzner–Otto constant. The Metzner–Otto constant k_s was determined through the experimental calibration for RT and PBRT$_D$ to obtain the values of 11.5 and 11.2, respectively.

2.2.2. Measurement of power consumption

During the experiment, the rotational speeds of impellers were adjusted through the console, and the corresponding torques of impellers were measured through the equipped torque sensor (HX-901, Huaxin Electromechanical Co., Ltd., China). These data can be recorded and saved in real time for subsequent data processing and analysis. In order to make the measured values more accurate, the torque was measured under load ($M_{l,l}$, $M_{r,l}$) and without load ($M_{l,0}$, $M_{r,0}$), respectively. All torque tests were repeated at least three times to eliminate accidental errors. The power consumption of the dual-shaft eccentric mixers can be calculated using the following formulas.

$$P = P_l + P_r \tag{4}$$

$$P_l = 2\pi N_l M_l \tag{5}$$

$$P_{\mathrm{r}} = 2\pi N_{\mathrm{r}} M_{\mathrm{r}} \tag{6}$$

$$M_l = M_{l,l} - M_{l,0} \tag{7}$$

$$M_{\mathrm{r}} = M_{\mathrm{r},l} - M_{\mathrm{r},0} \tag{8}$$

where P_l and P_{r} are the power consumption of the left impeller and the right impeller, respectively, and M_l and M_{r} are the torque of the left impeller and the right impeller, respectively. Power number (N_{P}) is an important parameter representing the mixing power. N_{P} is calculated as

$$N_{\mathrm{P}} = \frac{P}{\rho N^3 D^5} \tag{9}$$

2.2.3. Measurement of mixing time (t_m)

The mixing rate is an important indicator in industrial production because it reflects the time required to complete the mixing process. Fig. 2 shows the feed point (P_0) of the tracer and five monitoring points (P_1–P_5). Numerical simulations are employed to track the dispersion of the tracer in order to estimate the mixing time [43,44]. The determination of mixing time (t_{m}) followed the 95% principle, which is consistent with our previous research [22,23].

3. Numerical Methodology

3.1. Theoretical basis and boundary conditions

In this simulation work, the flow medium was a single-phase, isothermal, and incompressible flow of CMC inside the stirred tank. The rotational speed was set between 60 and 300 $\mathrm{r \cdot min^{-1}}$ in the CFD calculation, with the corresponding Reynolds numbers (Re^*) ranging from 27.75 to 169.42. The laminar flow model was employed to simulate the mixing of CMC solutions [2,24]. The continuity and momentum equations were solved both separately and simultaneously.

The mass conservation equation [45] of the flow model is

$$\frac{\partial \rho}{\partial t} + \frac{\partial(\rho u)}{\partial x} + \frac{\partial(\rho v)}{\partial y} + \frac{\partial(\rho w)}{\partial z} = 0 \tag{10}$$

where ρ is the fluid density; t is the flow time; and u, v and w are velocity components in x, y and z directions.

Momentum conservation equations [45] are as follows:

$$\frac{\partial \rho u}{\partial t} + \nabla \cdot (\rho u \boldsymbol{V}) = -\frac{\partial p}{\partial x} + \frac{\partial \tau_{xx}}{\partial x} + \frac{\partial \tau_{yx}}{\partial y} + \frac{\partial \tau_{zx}}{\partial z} + F_x \tag{11}$$

$$\frac{\partial \rho v}{\partial t} + \nabla \cdot (\rho v \boldsymbol{V}) = -\frac{\partial p}{\partial y} + \frac{\partial \tau_{xy}}{\partial x} + \frac{\partial \tau_{yy}}{\partial y} + \frac{\partial \tau_{zy}}{\partial z} + F_y \tag{12}$$

$$\frac{\partial \rho w}{\partial t} + \nabla \cdot (\rho w \boldsymbol{V}) = -\frac{\partial p}{\partial z} + \frac{\partial \tau_{xz}}{\partial x} + \frac{\partial \tau_{yz}}{\partial y} + \frac{\partial \tau_{zz}}{\partial z} + F_z \tag{13}$$

where F_x, F_y and F_z are the stresses received by the fluid element in the x, y and z directions, respectively. When the stress is gravity only, $F_x = 0$, $F_y = 0$ and $F_z = -\rho g$.

The commercial CFD package, Fluent 2020 R2, was used in this study. The baffles and impeller blades were considered zero-thickness walls. The entire flow region was divided into two regions: the moving region and the stator region. Furthermore, the refined mesh was employed near the impeller and wall to account for the significant velocity gradient in those areas. The model adopted in this study was consistent with our previous work, and more detailed information can be found in the referenced previous studies [23]. Specific meshing is shown in Fig. 3.

The multiple reference frame (MRF) model and sliding mesh (SM) model were utilized to address the rotation of the impellers in both steady-state and transient motion calculations. In this approach, the steady-state calculation results served as the initial flow field conditions for the SM model. This integration of MRF and SM models enabled an effective simulation of the impeller rotation

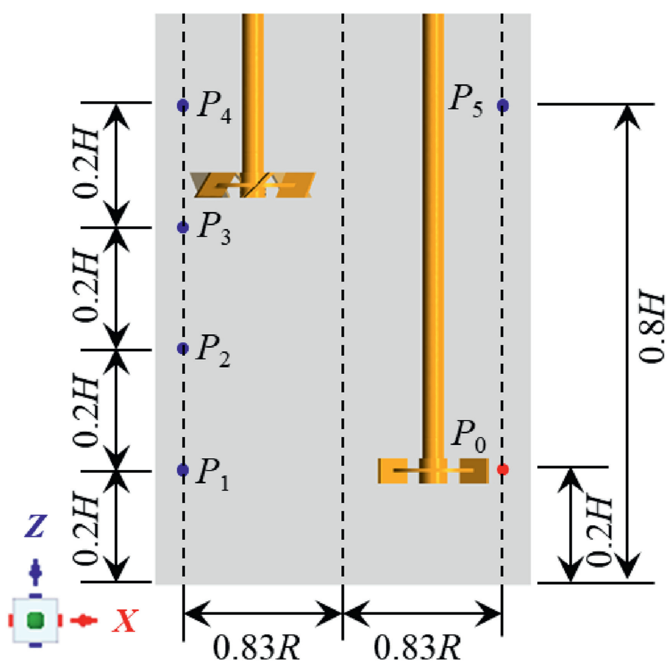

Fig. 2. The location diagram of tracer feed point and five monitoring points.

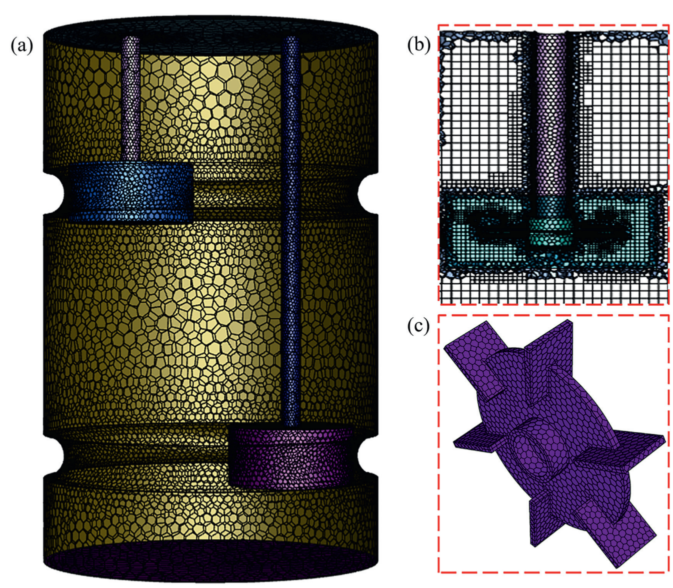

Fig. 3. Computational grids: (a) stirred tank; (b) refined mesh of interface, impeller and shaft; (c) impeller.

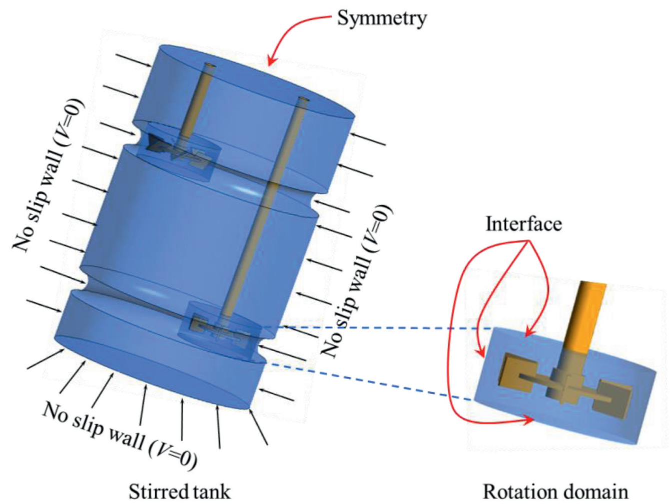

Fig. 4. Boundary conditions of the stirred tank.

and ensured accurate predictions of flow behavior. A second-order upwind discretization scheme was employed to calculate the momentum equations. At the liquid surface, all normal gradients were set to zero, representing the symmetry boundary. The pressure–velocity coupling was achieved using the SIMPLE algorithm [27,30]. The coincident surfaces between the moving zone and stator zone were defined as "interface". The tank wall, shaft, and impellers were all treated as no-slip wall boundaries. Within the moving zone, the impeller and shaft were assigned a zero speed relative to the adjacent cell zone, while the rotor shaft outside the moving zone was set to match the absolute impeller speed. Fig. 4 shows the specific boundary conditions of the stirred tank. Convergence residuals for each equation were set to 1×10^{-5}.

3.2. Validation of computational model

The accuracy of the model was verified by a power consumption experiment with CMC fluids. Fig. 5 shows the experimental and simulated power consumption values of a standard baffle mixing system at different rotational speeds. We found that the experimental values agree well with the simulated values, which proved the accuracy of the laminar flow model established in this study.

4. Results and Discussion

4.1. Power consumption

Power consumption is one of the key concerns in industrial mixing production. Fig. 6 shows the power curve against Reynolds number (*Re*) for three different mixing systems. The power curve of three systems shows the following: (1) *P* increased continuously with the increase of *Re* in all mixing systems. With the same Reynolds number, the power numbers show little difference in the laminar flow. This means that the baffle types have no effect on power consumption as the impeller speed is low in laminar flow. (2) In the transitional flow ($Re > 60$), the fluid speed of the baffle region becomes relatively high with the impeller rotational speed increasing, and the interaction between the baffle and tangential flow affects the impeller region, influencing its power consumption. Compared to standard baffle mixing systems, the power number of both unbaffle and U-shaped baffle systems is decreased under the same conditions. Due to the additional resistance of the baffle to the tangential flow generated by the impeller, power consumption is increased. To find the inherent mechanism behind the mass transfer performances in different mixing systems, the comparison of velocity flow behaviors in different systems has been studied in the next section.

4.2. Velocity distribution

The velocity distributions of three mixing tanks at 300 $r \cdot min^{-1}$ is showed in Fig. 7. As shown in Fig. 7(a) and (b), we have divided the tank into three areas: the upper area (part A), the middle area (part B), and the lower area (part C). Compared with the baffle tank and the unbaffle tank, the mixing tank equipped with a U-shaped baffle can strengthen the fluid circulation in the whole tank, and the overall velocity distribution is more homogeneous. It is worth noting that the lower impeller

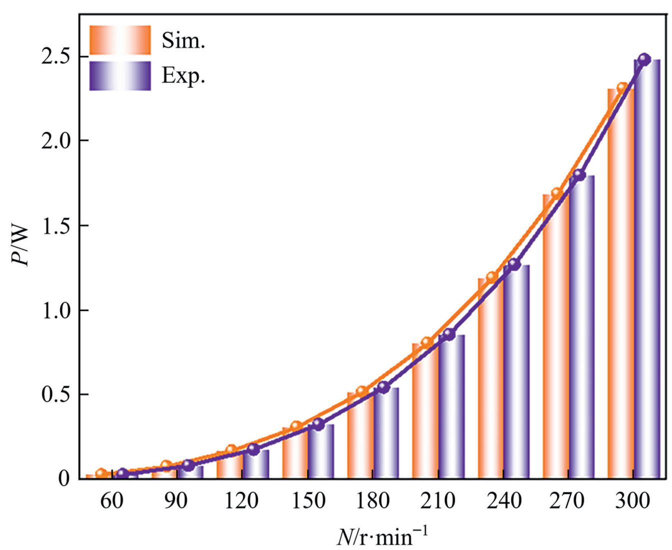

Fig. 5. CFD model predicted power consumption with experimental date in the standard baffle mixing system.

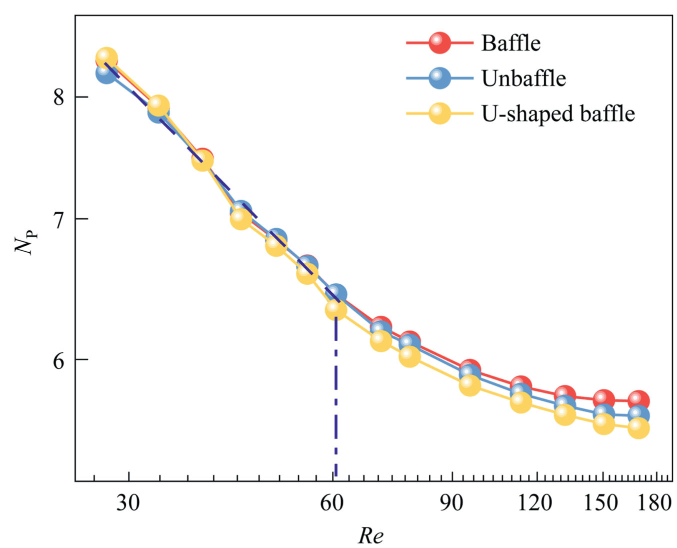

Fig. 6. Power curve against Reynolds for different mixing systems.

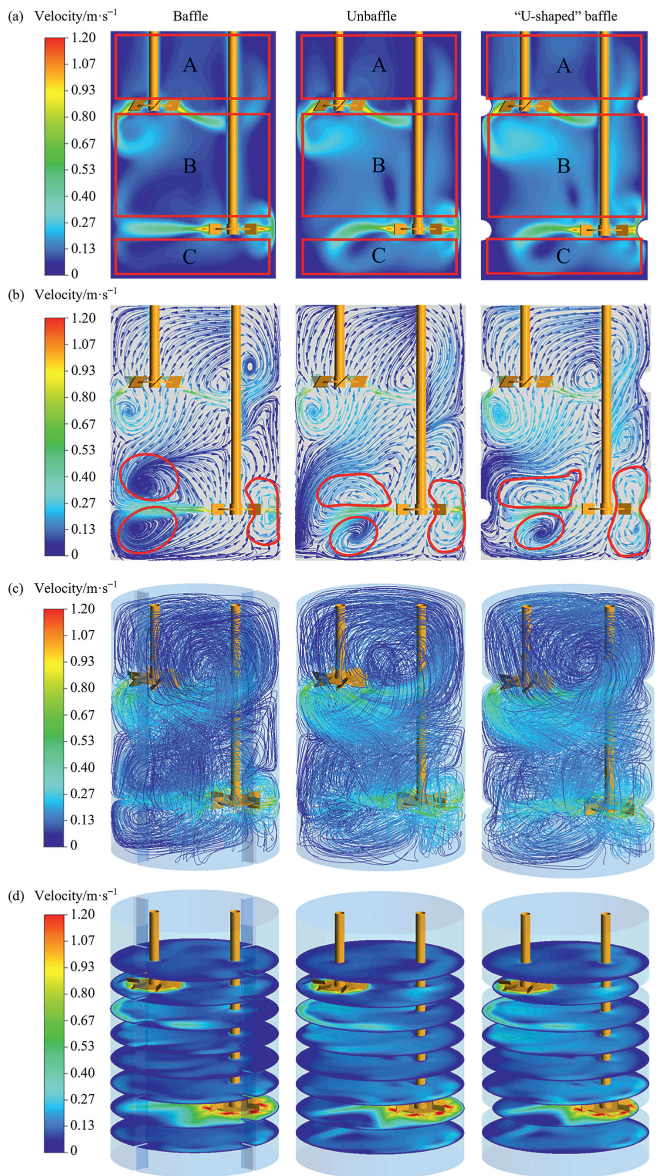

Fig. 7. Velocity distributions of different mixing tanks at 300 $r\cdot min^{-1}$: (a) velocity contours, (b) velocity vectors, (c) 3D streamlines, (d) velocity contours of cross-section.

of the unbaffle and U-shaped baffle tank pumps the fluid in an inclined direction, which enhances the stretching and folding of the fluid and enlarges the chaotic mixing region of the lower area fluid. On the contrary, the 3D streamlines in the lower area of the baffle stirred tank form two vortexes, which prevent the circulation of fluid (as shown in Fig. 7(b) and (c)). Furthermore, the distribution of fluid kinetic energy at the position of the U-shaped baffle is controlled directionally. The sudden drop of instantaneous incoming flow speed at this position causes a sharp reduction of kinetic energy, which is partially converted into pulsating kinetic energy and pressure pulse, and strengthens the uniform distribution of fluid velocity. As expected, Fig. 7(d) demonstrated a wider spatial distribution of velocities in the U-shaped baffle mixing tanks.

Fig. 8 shows the statistical distribution of velocity at different times in three stirred tanks. With the prolongation of mixing time, the fluid velocity distributions of the three mixing systems gradually converge to a steady state. As shown in Fig. 8(a), there is no obvious change in the baffled mixing tank, and the maximum dimensionless velocity is 0.1. The baffle mixing tank's dimensionless velocity distribution changes with the mixing time's prolongation until it reaches the steady state. Maximum dimensionless velocity in the mixing tank in the range of 0.2–0.3 indicates a more uniform velocity distribution of the fluid. Based on the reinforcing effect of the U-shaped baffle, the maximum dimensionless fluid velocity further increases to close to 0.3. This is in good agreement with the conclusions obtained for Fig. 7.

To further reveal the kinetic energy distribution mechanism of the stirred tank modulated by different baffle configurations and structures, we extracted the distributions of *X*-directional velocity and total velocity separately on 24 cross-sections perpendicular to the shaft in three mixing systems, as shown in Figs. 9 and 10, respectively.

As shown in Fig. 9, the overall distribution of *X*-direction velocity is similar for all three mixing systems at low rotational speeds ($N = 120$ $r\cdot min^{-1}$), while the velocity is maximum for the U-shaped baffle mixing system in the impeller regions. As the rotational speed increases to 210 $r\cdot min^{-1}$, the advantage of the U-shaped baffle system for the distribution of the velocity regulation in the bottom and top regions of the tank becomes evident. At 300 $r\cdot min^{-1}$, we find the lowest *X*-direction velocity in the bottom region of the unbaffle mixing tank, while the mixing system equipped with the baffle in the upper region has a low velocity. In addition, there is no significant difference in the middle area of the impellers between the three mixing systems at different rotational speeds.

Fig. 10 indicates that at low rotational speeds ($N = 120$ $r\cdot min^{-1}$), compared with baffle and unbaffle mixing systems, the U-shaped baffle mixing tank only enhances the velocity distribution in the impeller area. As the rotational speed increases, the advantage of the U-shaped baffle to regulate the velocity distribution of the whole mixing tank becomes more obvious, especially in the region between the $PBRT_D$ impeller and the RT impeller. This demonstrates the importance of the strategy for modulating control of the kinetic energy distribution to enhance the fluid velocity distribution in the tanks.

4.3. Average shear rate

Fig. 11 shows the average strain rate at the vertical section in three mixing systems at $N = 300$ $r\cdot min^{-1}$. Results showed that the larger shear strain rate was mainly concentrated near the impeller region, while the smaller shear strain rate was in the upper and lower regions of the tank. It is worth noting that the range of the average shear rate distribution in the middle region of the impellers in the U-shaped baffle tank is larger compared to the baffle and unbaffle tanks. A quantitative analysis of the three mixing systems comparison will follow to further determine the reasons for the superiority of the U-shaped baffle mixing system.

Fig. 12 shows the average shear rate separately on 24 cross-sections perpendicular to the shaft in three mixing systems. It can be observed that the overall average shear strain rate in the tank increases with the increase in rotational speed. At the same speed, the average shear rate of the baffle and unbaffle tanks is close. The reason is that the vertical standard baffle has less influence on the fluid in laminar flow. In addition, it can be found that the U-baffle mixing system can strengthen the average shear rate distribution in the whole tank, especially for the height of the two blades, which is significantly higher than that of the baffle and unbaffle stirred tanks.

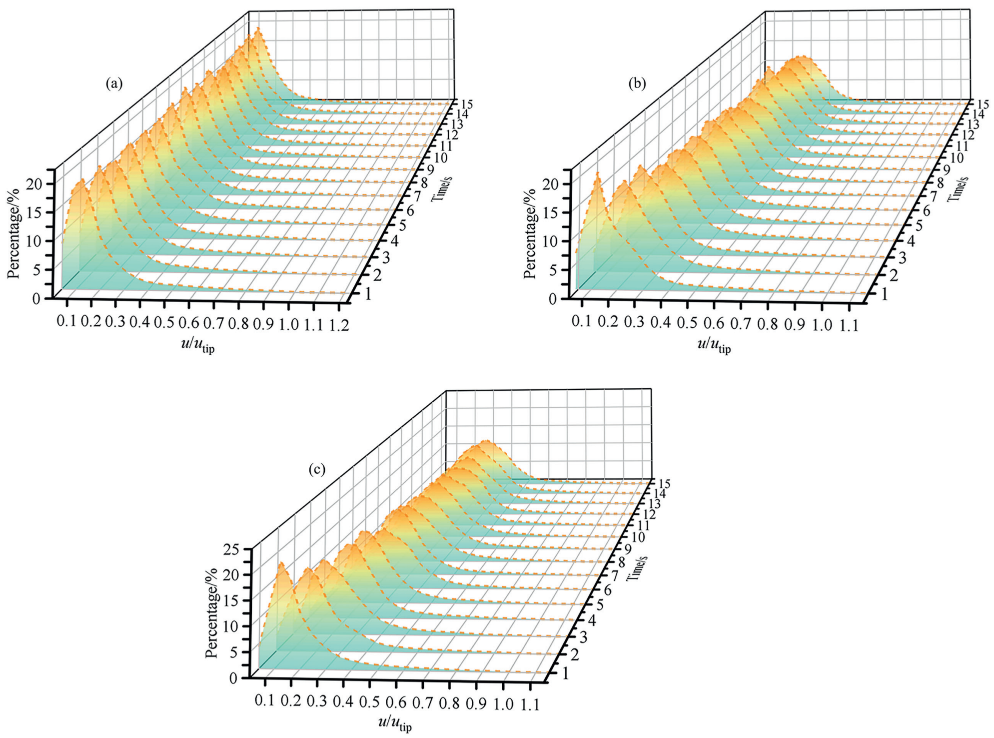

Fig. 8. Statistical distributions of velocity at different times in three stirred tanks at 300 r·min^{-1}: (a) baffle, (b) unbaffle, (c) U-shaped baffle.

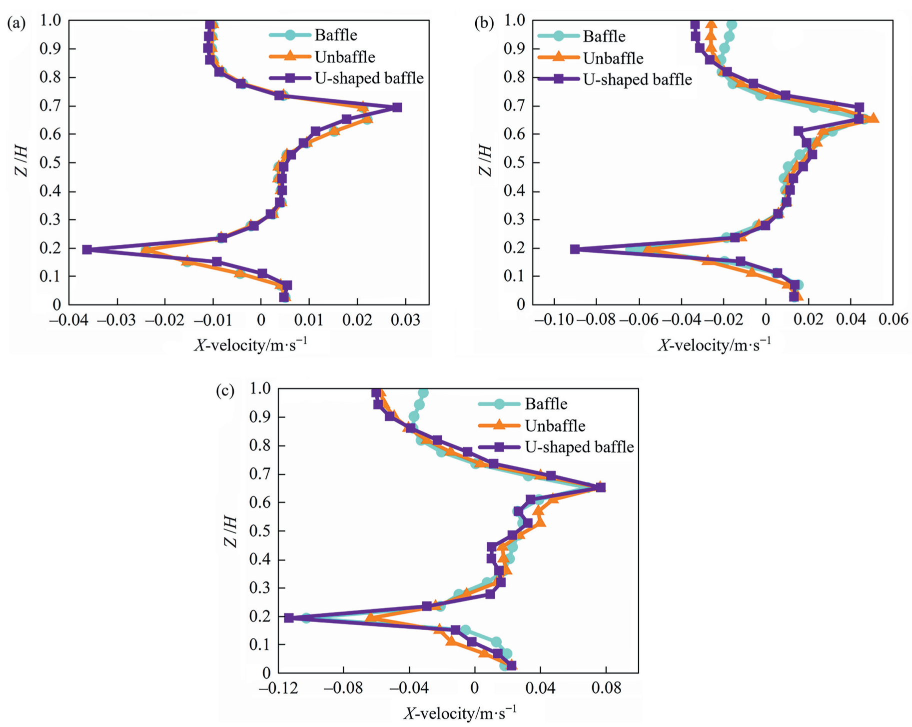

Fig. 9. Distributions of X-directional velocity at axial direction in three mixing systems: (a) 120 r·min^{-1}, (b) 210 r·min^{-1}, (c) 300 r·min^{-1}.

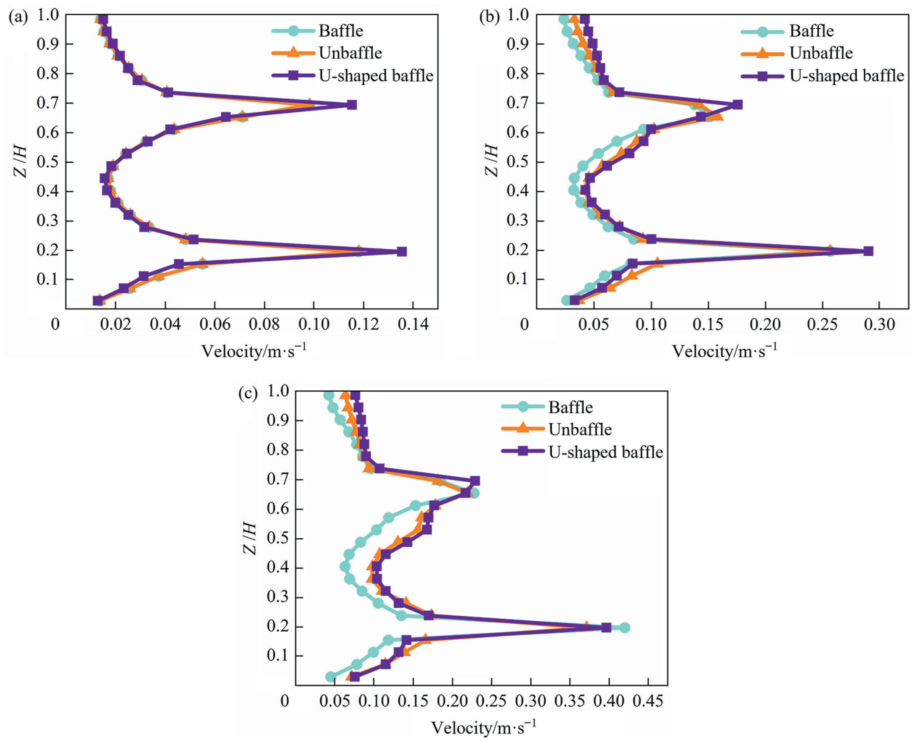

Fig. 10. Distributions of velocity at axial direction in three mixing systems: (a) 120 r·min^{-1}, (b) 210 r·min^{-1}, (c) 300 r·min^{-1}.

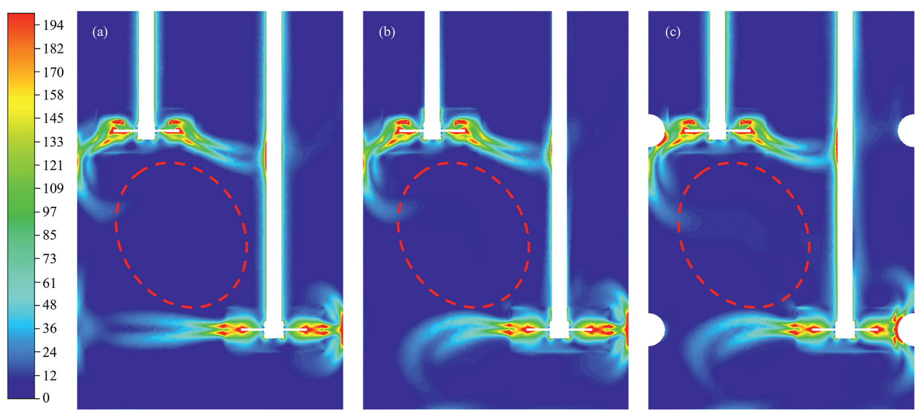

Fig. 11. Distributions of average strain rate at vertical section in three mixing systems: (a) baffle, (b) unbaffle, (c) U-shaped baffle.

Fig. 13 shows the distribution of average strain rate at the height of impellers in three mixing systems. At the height of the impellers, the average shear rate is highest in the U-shape baffle mixing systems compared to the baffle and unbaffle systems. Specifically, at $N = 300$ r·min^{-1}, the average strain rate of a U-shaped baffle tank was 13.8% and 16.1% higher than that of baffle and unbaffle tanks at $Z/H = 0.2$, respectively, while it was higher than that of baffle and unbaffle tanks (22.1% and 27.7%, respectively, $Z/H = 0.7$). Besides, as the mixing speed increases, the advantage of the U-shaped baffle stirred tank reinforced localized region of fluid stretching and folding becomes more obvious.

4.4. Mixing performance

Fig. 14 shows the variation in the dimensionless concentration of the liquid tracer over time. The curves of the unbaffled stirred tank are the smoothest, and those of the U-shaped baffle stirred tank are the most erratic. In each system, the dimensionless concentration curves gradually converged to stable values over time. Additionally, in all three tanks, the last one to achieve 95% uniformity was monitoring the P_5 solution at the liquid surface. Results show that the t_m of the baffle, unbaffle and U-shaped baffle tanks are 13.61, 13.12 and 11.38 s, respectively. It can be found that the presence or absence of a standard baffle has little influence on the mixing time of non-Newtonian fluid under the same conditions. The t_m of the U-shaped baffle tank was nearly 16.4% and 13.3% shorter than that of the baffle and unbaffle tanks, respectively. It indicated that U-shaped baffles can effectively shorten the mixing time.

Fig. 15(a) shows the relationship between the mixing time (t_m) and power consumption per unit volume (P_v). It can be observed that the mixing time unsurprisingly decreased with the increase

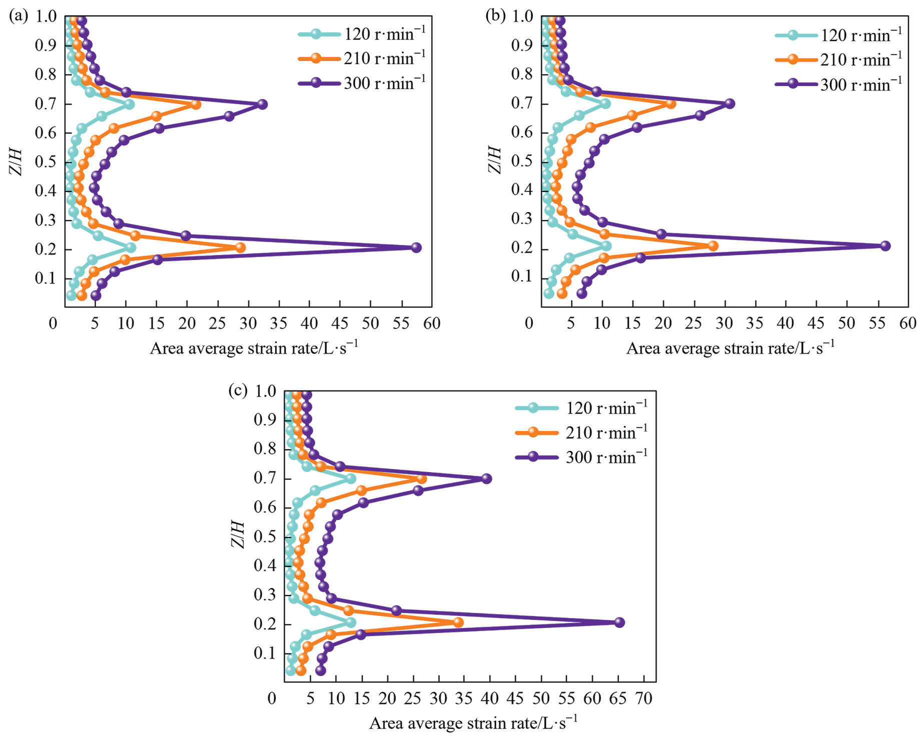

Fig. 12. Distributions of average strain rate at axial direction in three mixing systems: (a) baffle, (b) unbaffle, (c) U-shaped baffle.

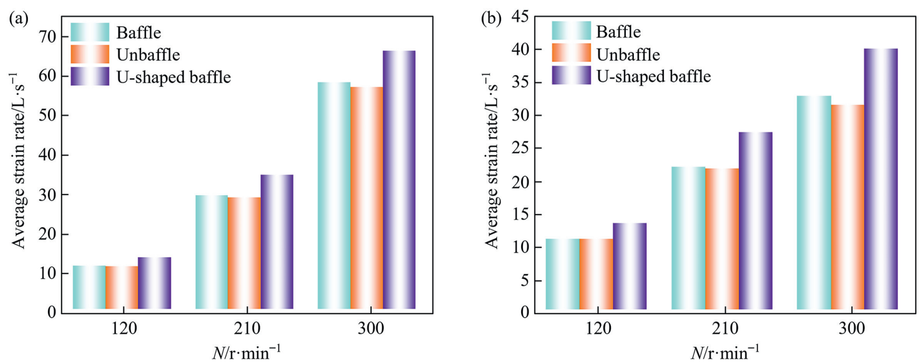

Fig. 13. Distributions of average strain rate at height of impellers in three mixing systems: (a) $Z/H = 0.2$, (b) $Z/H = 0.7$.

of P_v in all three systems. Furthermore, at the same P_v, the longest mixing time appeared in the standard baffle mixing system, followed by the unbaffle and U-shaped baffle mixing systems (baffle > unbaffle > U-shaped baffle). This can be attributed to the fact that the U-shaped baffle accurately regulates the movement of the fluid field in the baffle region and enhances the nonlinear instability of the fluid in the whole tank. As illustrated in Fig. 15(b), at the same rotational condition, the values of mixing energy per unit volume (W_v) in the U-shaped baffle mixing system were lower than those in the standard baffle and unbaffle mixing systems, and the values of W_v could be further increased with the increase of P_v. Specifically, the W_v of U-shaped baffle systems was 15.6% and 10.1% lower than that of standard baffle and unbaffle mixing systems at $P_v = 0.07\ \text{kW}\cdot\text{m}^{-3}$, respectively. As the P_v increased to 0.14 kW, the W_v of the U-shaped baffle was 19.1% and 13.3% lower than that of the baffle and unbaffle systems, respectively. According to the mixing energy results, a reduction in the mixing time occurs at the expense of increasing power consumption. From the perspective of unit volume energy, the most energy-efficient non-Newtonian fluid mixing operation condition is low energy input, that is, low stirring speed. Hence, we recommend the use of U-shaped baffle mixers in industrial production involving non-Newtonian fluids due to their ability to achieve high energy efficiency while maintaining low power consumption.

Fig. 16 shows the dimensionless mixing time *versus* Reynolds number. As can be seen, the results show a linear relationship between the Reynolds number and Nt_m in three mixing systems. The fundamental implication is that a deliberate augmentation of the Reynolds number precipitates a concomitant escalation in the dimensionless mixing time. It is important to bear in mind that the rise in Reynolds number (Re) is solely attributed to the

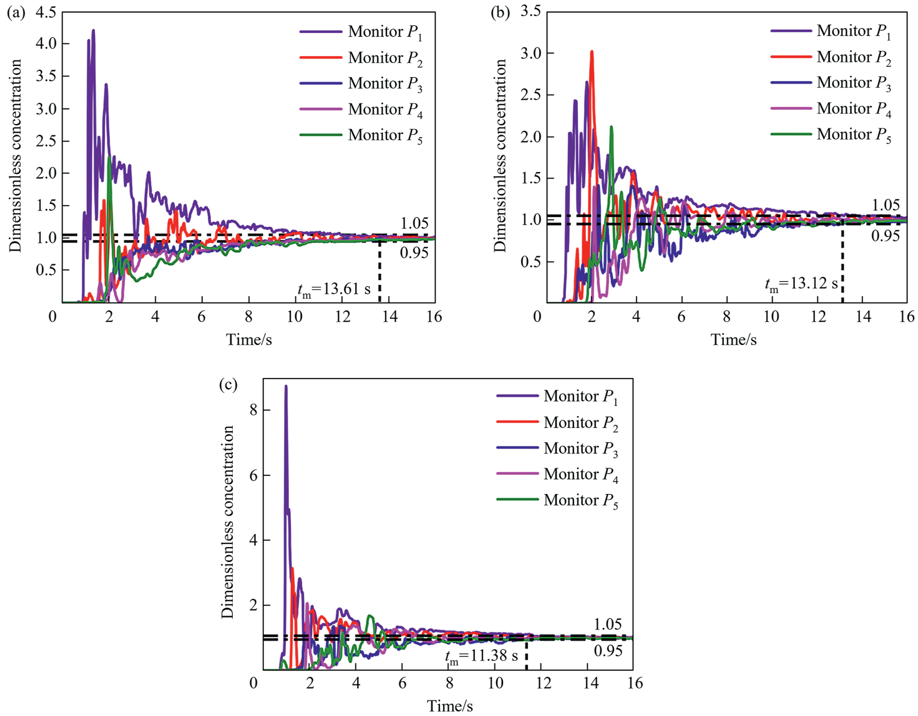

Fig. 14. Dimensionless concentrations of liquid tracer over time in three mixing systems: (a) baffle, (b) unbaffle, (c) U-shaped baffle.

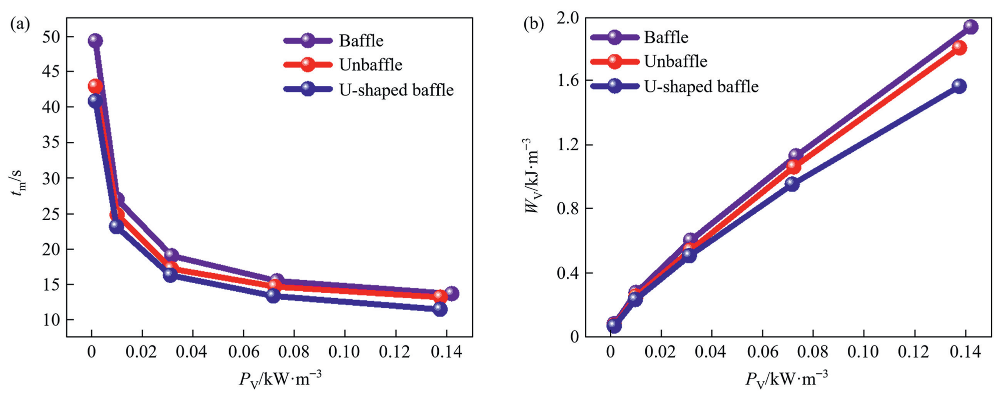

Fig. 15. Mixing time and mixing energy per unit volume against power consumption per unit volume for different mixing systems: (a) mixing time, (b) mixing energy per unit volume.

escalation in impeller rotational speed. However, this increase in speed exhibits limited efficacy in substantially diminishing the dimensionless mixing time. Further improvements are achieved by the increase in its rotational. At the same *Re*, the Nt_m of the U-shaped baffle system was nearly 15.3% and 7.9% shorter than that of standard baffle and unbaffle mixing systems, respectively. It indicated that U-shaped baffle systems can shorten mixing time on the basis of the same stirred condition. The advantages of U-shaped baffle systems in terms of mixing rate were illustrated.

4.5. Fluid transport mechanism

Fig. 17 shows the fluid transport mechanism of three mixing systems. As shown in Fig. 17(a), fluid transportation in the wall region was hindered by the baffles, resulting in the formation of high-velocity vortex zones in the near-impeller region, which increased the fluid velocity between impeller and wall and enhanced the local region's chaotic mixing. Unfortunately, multiple low-velocity isolated regions were formed in the lower part of the tank, which was inefficient and unfavorable in terms of momentum and mass exchange. For the unbaffled mixing system (Fig. 17(b)), the low-velocity vortex regions gradually disappear, and the overall flow field has a more uniform velocity distribution. However, the flow velocity of fluid in the wall region was still low, which clearly requires further optimization of the wall structure to enhance the chaotic mixing of the local fluid. Unsurprisingly, the proposed U-shaped baffle solved the above problems (Fig. 17(c)), which accelerated the fluid transport process on the wall surface through the special U-shaped

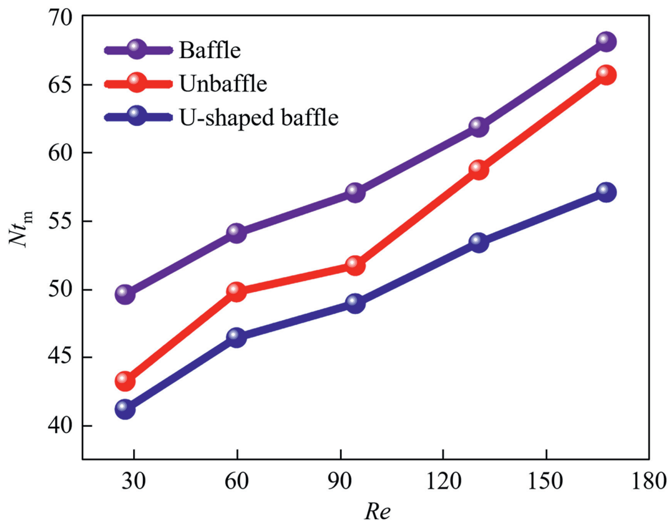

Fig. 16. The dimensionless mixing time *versus* Reynolds number for the three different mixing systems.

structure, making the fluid flow pattern from radial flow to axial flow rapid transformation, and strengthening the stretching and folding process of non-Newtonian fluid. In turn, it regulates the fluid in the whole tank and makes its velocity distribution more uniform.

5. Conclusions

In summary, this work proposes an innovative approach that changes the kinetic energy of the fluid by embedding U-shaped annular baffles on the wall of the stirred tank, thereby controlling and generating different axial and radial flow patterns. Firstly, the power consumption characteristics of three different mixing systems (baffle, unbaffle and U-shaped baffle mixing systems) are compared. Under the same rotational conditions, the power number of the laminar flow state remains relatively consistent, while the power number of both unbaffle and U-shaped annular baffle mixing systems decreases compared with the standard baffle mixing system in the transition flow. In addition, *via* analysis of the magnitude and distribution of the velocity and average shear rate, the U-shaped baffle can change the flow field pattern of the fluid in the tank, strengthen the stretching and folding of the fluid in the local region of the baffle, and accelerate the fluid transport process in the wall area, so as to regulate the uniform distribution of the fluid velocity and shear rate in the whole tank. Finally, a conventional strategy for controllable flow pattern generation based on dual-shaft stirring coupled with a U-shaped baffle is proposed. In the future, our aim is to develop comprehensive models for non-Newtonian fluid mixing encompassing a range of U-shaped structural configurations.

Declaration of Interest

The authors declare that they have no known competing financial interests or personal relationships that could have appeared to influence the work reported in this paper.

Acknowledgements

This work was supported by the National Natural Science Foundation of China (22078030, 52021004), Natural Science Foundation of Chongqing (2022NSCO-LZX0014), Fundamental Research Funds for the Central Universities (2022CDJQY-005, 2023CDJXY-047), National Key Research and Development Project (2022YFC3901204).

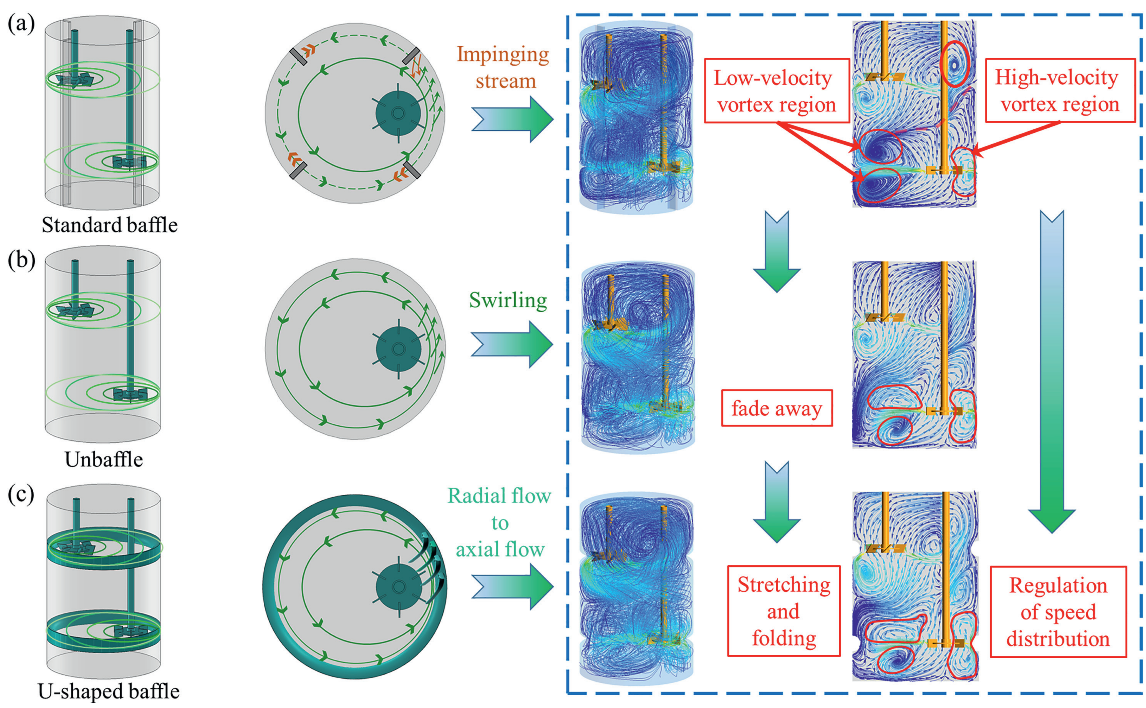

Fig. 17. Schematic diagrams of fluid transport mechanism: (a) standard baffle mixing system, (b) unbaffle mixing system, (c) U-shaped baffle mixing system.

Nomenclature

b	impeller blade width, m
C_1	off-bottom clearance of left impeller, m
C_2	off-bottom clearance of right impeller, m
D	impeller diameter, m
D_d	disc diameter of impeller, m
d	U-shaped baffle height, m
e	eccentric distance, m
H	fluid height, m
K	consistency index, $Pa \cdot s^n$
k_s	constant of Metzner–Otto
M	torque, $N \cdot m$
N	impeller speed, $r \cdot s^{-1}$
n	rheological index
P	power consumption, W
r	U-shaped baffle radius, m
T	vessel diameter, m
t_m	mixing time, s
V	fluid volume, m^3
w	baffle width, m
w_t	mass fraction
$\dot{\gamma}$	shear rate, s^{-1}
η	non-Newtonian viscosity, $Pa \cdot s$
μ_a	apparent viscosity, $Pa \cdot s$
ρ	density, $kg \cdot m^{-3}$
τ	shear stress, Pa

Subscripts

l	left
r	right

References

[1] S. Foucault, G. Ascanio, P.A. Tanguy, Power characteristics in coaxial mixing: Newtonian and non-Newtonian fluids, *Ind. Eng. Chem. Res.* 44 (14) (2005) 5036–5043.
[2] P. Wang, T. Reviol, S. Kluck, P. Würtz, M. Böhle, Mixing of non-Newtonian fluids in a cylindrical stirred vessel equipped with a novel side-entry propeller, *Chem. Eng. Sci.* 190 (2018) 384–395.
[3] J.S. Ayala, H.L. de Moura, R. de Lima Amaral, F. de Assis Oliveira Jr., J.R. Nunhez, G.J. de Castilho, Two-dimensional shear rate field and flow structures of a pseudoplastic fluid in a stirred tank using particle image velocimetry, *Chem. Eng. Sci.* 248 (2022) 117198.
[4] S. Saeed, F. Ein-Mozaffari, S.R. Upreti, Using computational fluid dynamics to study the dynamic behavior of the continuous mixing of Herschel–Bulkley fluids, *Ind. Eng. Chem. Res.* 47 (19) (2008) 7465–7475.
[5] M. Zlokarnik, Stirring: Theory and Practice, Wiley-VCH, Weinhim, 2001.
[6] L. Pakzad, F. Ein-Mozaffari, P. Chan, Using electrical resistance tomography and computational fluid dynamics modeling to study the formation of cavern in the mixing of pseudoplastic fluids possessing yield stress, *Chem. Eng. Sci.* 63 (9) (2008) 2508–2522.
[7] P. Prajapati, F. Ein-Mozaffari, CFD investigation of the mixing of yield-pseudoplastic fluids with anchor impellers, *Chem. Eng. Technol.* 32 (8) (2009) 1211–1218.
[8] L. Rudolph, M. Schäfer, V. Atiemo-Obeng, M. Kraume, Experimental and numerical analysis of power consumption for mixing of high viscosity fluids with a co-axial mixer, *Chem. Eng. Res. Des.* 85 (5) (2007) 568–575.
[9] H. Aref, Stirring by chaotic advection, *J. Fluid Mech.* 143 (1984) 1–21.
[10] J.M. Ottino, The Kinematics of Mixing: Stretching, Chaos and Transport, Cambridge University Press, Cambridge, 1989.
[11] G.O. Fountain, D.V. Khakhar, J.M. Ottino, Visualization of three-dimensional chaos, *Science* 281 (5377) (1998) 683–686.
[12] M.M. Alvarez-Hernández, T. Shinbrot, J. Zalc, F.J. Muzzio, Practical chaotic mixing, *Chem. Eng. Sci.* 57 (17) (2002) 3749–3753.
[13] D.R. Gao, M.J. Guo, Y. Li, Z.L. Fan, PIV experimental investigation of chaotic mixing using non-constant speed stirring, *Chin. J. Mech. Eng.* 42 (8) (2006) 44–49. (in Chinese)
[14] S. Woziwodzki, Turbulent forward–reverse mixing characteristics in vessel with multiple-turbine impellers, *J. Chem. Technol. Biot.* 88 (3) (2013) 483–490.
[15] X. Xiong, S.S. Wang, P.Q. Liu, C.Y. Tao, Y.D. Wang, Z.H. Liu, Numerical investigation on intensified mixing performance with modified dual impeller, *Chem. Eng. Sci.* 274 (2023) 118698.
[16] D.Y. Gu, Z.H. Liu, Z.M. Xie, J. Li, C.Y. Tao, Y.D. Wang, Numerical simulation of solid–liquid suspension in a stirred tank with a dual punched rigid-flexible impeller, *Adv. Powder Technol.* 28 (10) (2017) 2723–2734.
[17] Z.H. Liu, X.Y. Yang, Z.M. Xie, R.L. Liu, C.Y. Tao, Y.D. Wang, Chaotic mixing performance of high-viscosity fluid synergistically intensified by flexible impeller and floating particles, *CIESC Journal* 64 (8) (2013) 2794–2800. (in Chinese)
[18] K.C. Ng, E.Y.K. Ng, Laminar mixing performances of baffling, shaft eccentricity and unsteady mixing in a cylindrical vessel, *Chem. Eng. Sci.* 104 (2013) 960–974.
[19] M.M. Alvarez, P.E. Arratia, F.J. Muzzio, Laminar mixing in eccentric stirred tank systems, *Can. J. Chem. Eng.* 80 (4) (2002) 546–557.
[20] B. Letellier, C. Xuereb, P. Swaels, P. Hobbes, J. Bertrand, Scale-up in laminar and transient regimes of a multi-stage stirrer, A CFD approach, *Chem. Eng. Sci.* 57 (21) (2002) 4617–4632.
[21] D.Y. Luan, S.F. Zhang, X. Wei, Z.Y. Duan, Effect of the 6PBT stirrer eccentricity and off-bottom clearance on mixing of pseudoplastic fluid in a stirred tank, *Results Phys.* 7 (2017) 1079–1085.
[22] S.S. Wang, H. Li, C.Y. Tao, R.L. Liu, Y.D. Wang, Z.H. Liu, Study on cavern evolution and performance of three mixers in agitation of yield-pseudoplastic fluids, *Chin. J. Chem. Eng.* 55 (2023) 111–122.
[23] S.S. Wang, X. Xiong, P.Q. Liu, Q.Z. Zhang, Q. Zhang, C.Y. Tao, Y.D. Wang, Z.H. Liu, CFD simulation of hydrodynamics and mixing performance in dual shaft eccentric mixers, *Chin. J. Chem. Eng.* 62 (2023) 297–309.
[24] L. Pakzad, F. Ein-Mozaffari, S.R. Upreti, A. Lohi, Evaluation of the mixing of non-Newtonian biopolymer solutions in the reactors equipped with the coaxial mixers through tomography and CFD, *Chem. Eng. J.* 215–216 (2013) 279–296.
[25] D.Y. Luan, Y.M. Chen, H. Wang, Z.R. Wang, S.S. Wang, L.B. Li, Formation of heart-shaped cavern model in stirring pseudoplastic fluid with the impeller of perturbed six-bend-blade turbine, *AIChE J.* 65 (5) (2019) e16572.
[26] D.Y. Luan, Z.R. Wang, H. Wang, S.S. Wang, L.B. Li, Y.M. Chen, Determination method of the cavern boundary viscosity in a stirred tank with pseudoplastic fluid, *AIChE J.* 66 (5) (2020) e16941.
[27] F.L. Yang, C.X. Zhang, T.L. Su, Power and flow characteristics of flexible-blade Rushton impeller, *CIESC Journal* 71 (2) (2020) 614–625. (in Chinese)
[28] D.Y. Gu, J. Wang, H. Yang, Y.Y. Deng, Investigation on solid particles and pseudoplastic fluid mixing characteristics in a dislocated self-similarity impeller stirred reactor, *Ind. Eng. Chem. Res.* 62 (27) (2023) 10700–10710.
[29] D.Y. Gu, T. Yang, L.F. Xie, Mixing characteristics of shear-thinning fluids in a fractal perforating impeller stirred reactor, *Ind. Eng. Chem. Res.* 62 (28) (2023) 11194–11205.
[30] P.C. Luo, J. Wu, X. Pan, Y.Q. Zhang, H. Wu, Gas–liquid mass transfer behavior in a surface-aerated vessel stirred by a novel long-short blades agitator, *AIChE J.* 62 (4) (2016) 1322–1330.
[31] M. Kordas, G. Story, M. Konopacki, R. Rakoczy, Study of mixing time in a liquid vessel with rotating and reciprocating agitator, *Ind. Eng. Chem. Res.* 52 (38) (2013) 13818–13828.
[32] Z. Zhang, G.R. Chen, Liquid mixing enhancement by chaotic perturbations in stirred tanks, *Chaos, Solit. Fractals* 36 (1) (2008) 144–149.
[33] D.J. Lamberto, F.J. Muzzio, P.D. Swanson, A.L. Tonkovich, Using time-dependent RPM to enhance mixing in stirred vessels, *Chem. Eng. Sci.* 51 (5) (1996) 733–741.
[34] F. Stręk, J. Karcz, Experimental studies of power consumption for agitated vessels equipped with non-standard baffles and high-speed agitator, *Chem. Eng. Process. Process. Intensif.* 32 (6) (1993) 349–357.
[35] F.L. Yang, S.J. Zhou, G.C. Wang, F.J. Hu, Study on the hydrodynamics of a stirred tank equipped with non-standard baffles, *J. Chem. Eng. Chin. Univ.* 26 (6) (2012) 952–958. (in Chinese)
[36] X.X. Wang, Z.Y. Liu, W.M. Long, D.F. Lyu, Research on flow field in elliptic bottom stirred tank with cruciform baffles, *Chin. J. Mech. Eng.* 50 (6) (2014) 156–164. (in Chinese)
[37] X. Xiong, Z.H. Liu, C.Y. Tao, Y.D. Wang, F.Q. Cheng, H. Li, Reduced power consumption in stirred vessel with high solid loading by equipping punched baffles, *Chin. J. Chem. Eng.* 56 (2023) 203–214.
[38] C. Sirasitthichoke, P.M. Armenante, Power dissipation and power number correlations for a retreat-blade impeller under different baffling conditions, *Ind. Eng. Chem. Res.* 56 (36) (2017) 10123–10133.
[39] V. Buwa, A. Dewan, A.F. Nassar, F. Durst, Fluid dynamics and mixing of single-phase flow in a stirred vessel with a grid disc impeller: Experimental and numerical investigations, *Chem. Eng. Sci.* 61 (9) (2006) 2815–2822.
[40] A. Kazemzadeh, F. Ein-Mozaffari, A. Lohi, L. Pakzad, Investigation of hydrodynamic performances of coaxial mixers in agitation of yield-pseudoplasitc fluids: Single and double central impellers in combination with the anchor, *Chem. Eng. J.* 294 (2016) 417–430.
[41] Y.Y. Bao, Y. Lu, Q.Q. Liang, L. Li, Z.M. Gao, X.B. Huang, S. Qin, Power demand and mixing performance of coaxial mixers in a stirred tank with CMC solution, *Chin. J. Chem. Eng.* 23 (4) (2015) 623–632.

[42] M.M. Buffo, L.J. Corrêa, M.N. Esperança, A.J.G. Cruz, C.S. Farinas, A.C. Badino, Influence of dual-impeller type and configuration on oxygen transfer, power consumption, and shear rate in a stirred tank bioreactor, *Biochem. Eng. J.* 114 (2016) 130–139.
[43] A. Paglianti, G. Montante, Simultaneous measurements of liquid velocity and tracer concentration in a continuous flow stirred tank, *Chem. Eng. Sci.* 216 (2020) 115495.
[44] Z. Jaworski, W. Bujalski, N. Otomo, A.W. Nienow, CFD study of homogenization with dual rushton turbines—Comparison with experimental results: Part I: Initial studies, *Chem. Eng. Res. Des.* 78 (3) (2000) 327–333.
[45] H.K. Versteeg, W. Malalasekera, An Introduction to Computational Fluid Dynamics: The Finite Volume Method, World Book Inc., Chicago, 2010.